

Importance of spin-orbit coupling in power factor calculations for half-Heusler ANiB (A=Ti, Hf, Sc, Y; B=Sn, Sb, Bi)

San-Dong Guo

Department of Physics, School of Sciences, China University of Mining and Technology, Xuzhou 221116, Jiangsu, China

We investigate the spin-orbit coupling (SOC) effects on the electronic structures and semi-classic transport coefficients of half-Heusler ANiB (A=Ti, Hf, Sc, Y; B=Sn, Sb, Bi) by using generalized gradient approximation (GGA). Calculated results show that SOC splits the valence bands at high symmetry Γ point, and modifies the outline of Γ -centered valence bands, which has remarkable effects on the electron transport properties. Thermoelectric properties are performed through solving Boltzmann transport equations within the constant scattering time approximation. It is found that the compounds containing Sn atom have larger power factor in p-type doping than ones in n-type doping, and it is just the opposite for compounds containing Sb and Bi elements. The SOC has obvious detrimental influence on power factor in p-type doping, while has a negligible effect in n-type doping. These can be understood by considering the effects of SOC on the valence bands and conduction bands. The maximum power factors (MPF) are extracted in n-type and p-type doping with GGA and GGA+SOC, and the MPF at 300 K with SOC is predicted to be about 4.25%~44.13% smaller than that without SOC in the case of p-type doping for ANiB (A=Ti, Hf, Sc, Y; B=Sn, Sb, Bi). Therefore, it is crucial to consider SOC effects for theoretical analysis in the case of p-type doping in half-Heusler compounds composed of heavy elements.

PACS numbers: 72.15.Jf, 71.20.-b, 71.70.Ej, 79.10.-n

Keywords: Half-Heusler; Spin-orbit coupling; Power factor

guosd@cumt.edu.cn

INTRODUCTION

Thermoelectric devices are potential energy converters to solve energy problems, which can convert waste heat directly to electricity using the Seebeck effect. The performance of thermoelectric material is characterized by the dimensionless thermoelectric figure of merit[1, 2], $ZT = S^2\sigma T/(\kappa_e + \kappa_L)$, where S , σ , T , κ_e and κ_L are the Seebeck coefficient, electrical conductivity, absolute working temperature, the electronic and lattice thermal conductivities, respectively. Many materials have been identified for thermoelectric applications, such as bismuth-tellurium systems[3, 4], silicon-germanium alloys[5, 6], lead chalcogenides[7, 8] and skutterudites[9, 10]. Heusler compounds have wide applications in spintronics, shape memory alloys, superconductors, topological insulators and thermoelectrics[11], and half-Heusler have attracted intensive research interest as moderate temperature thermoelectric materials due to being environmentally friendly, mechanically and thermally robust[12–18].

Recently, the transport properties of materials can be calculated accurately by combining the first principles band structure calculations and the Boltzmann transport theory[19–21]. Many theoretical simulation calculations have been performed for thermoelectric properties of half-Heusler[22–27]. However, most of them do not consider the SOC effects on transport properties. As is well known, spin-orbit interaction plays a key role in materials composed of heavy elements such as Bi or Sb, and SOC can induce topological insulators[28]. In ref.[29], relativistic effects in thermopower calculations for Mg_2X

(X=Si, Ge, Sn) are very remarkable, and have a detrimental influence on the thermoelectric performance of p-type Mg_2X . So, it is very necessary to know the SOC effects on the thermoelectric properties of half-Heusler compounds containing heavy elements.

Here, we investigate SOC effects on thermoelectric properties of half-Heusler ANiB (A=Ti, Hf, Sc, Y; B=Sn, Sb, Bi). It is found that SOC strongly affects the top valence bands near Γ point, which leads to a detrimental effect on p-type power factor. On the other hand, the SOC influence on conduction bands near the Fermi level is little, and a negligible SOC effect on n-type power factor is observed. At the presence of SOC, the MPF at 300 K is predicted to be about up to 44.13% smaller than that without SOC in the case of p-type doping for YNiBi. So, SOC is vital for the thermoelectric properties of half-Heusler compounds containing heavy element.

The rest of the paper is organized as follows. In the next section, we shall give our computational details. In the third section, we shall present our main calculated results and analysis. Finally, we shall give our conclusion in the fourth section.

COMPUTATIONAL DETAIL

We use a full-potential linearized augmented-plane-waves method within the density functional theory (DFT) [30], as implemented in the package WIEN2k [31]. We use the popular GGA[32] for the exchange-correlation potential to do our DFT calculations. The full relativistic effects are calculated with the Dirac equations for core states, and the scalar relativistic approx-

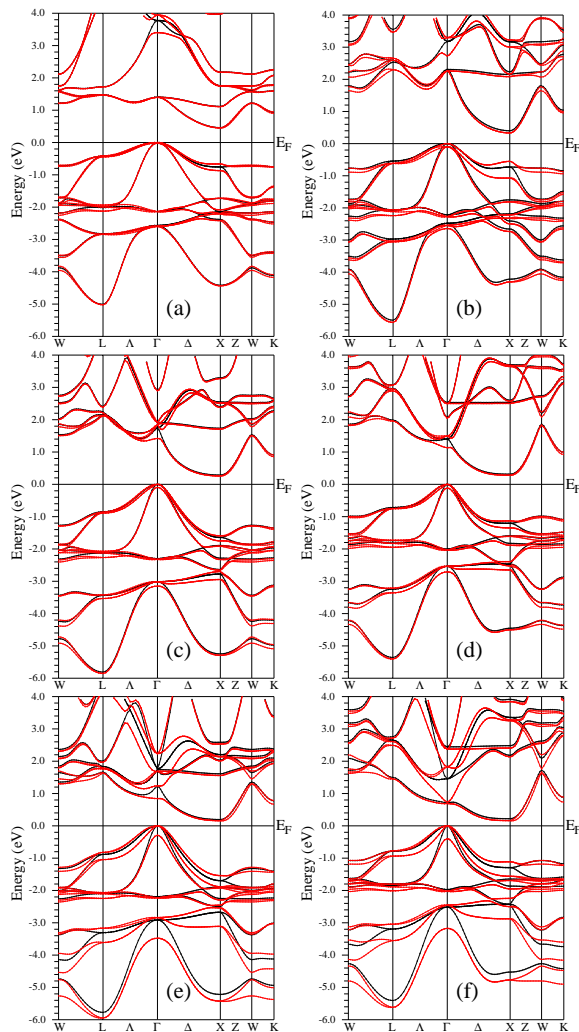


FIG. 1. (Color online) The energy band structures by using GGA (Black lines) and GGA+SOC (Red lines) (a) TiNiSn (b)HfNiSn (c) ScNiSb (d) YNiSb (e) ScNiBi (f) YNiBi.

imation is used for valence states [33–35]. The SOC was included self-consistently by solving the radial Dirac equation for the core electrons and evaluated by the second-variation method[36]. We use 5000 k-points in the first Brillouin zone for the self-consistent calculation. We make harmonic expansion up to $l_{\max} = 10$ in each of the atomic spheres, and set $R_{\text{mt}} \times k_{\max} = 8$. The self-consistent calculations are considered to be converged when the integration of the absolute charge-density difference between the input and output electron density is less than $0.0001|e|$ per formula unit, where e is the electron charge. Transport calculations are performed through solving Boltzmann transport equations within the constant scattering time approximation as implemented in BoltzTrap[21], which has been applied successfully to several materials[37–39]. To obtain accurate transport coefficients, we use 200000 k-points in the first Brillouin zone for the energy band calculation.

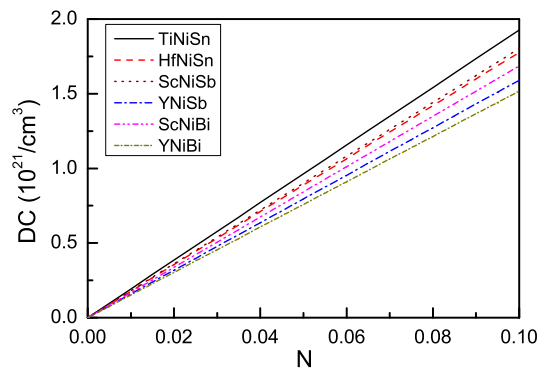


FIG. 2. (Color online) The corresponding relation between the doping concentration and electrons or holes per unit cell.

TABLE I. The experimental lattice constant a (Å); the calculated gap values with GGA E_1 (eV) and GGA+SOC E_2 (eV); $E_1 - E_2$ (eV); spin-orbit splitting Δ (eV) at the Γ point near the Fermi level in the valence bands. These values in the parentheses are GGA gaps in ref.[26].

| Name | a | E_1 | E_2 | $E_1 - E_2$ | Δ |
|--------|-------|---------------|-------|-------------|----------|
| TiNiSn | 5.921 | 0.460 (0.451) | 0.452 | 0.008 | 0.025 |
| HfNiSn | 6.084 | 0.401 (0.396) | 0.333 | 0.068 | 0.100 |
| ScNiSb | 6.055 | 0.286 (0.281) | 0.259 | 0.027 | 0.095 |
| YNiSb | 6.312 | 0.314 (0.311) | 0.281 | 0.033 | 0.117 |
| ScNiBi | 6.191 | 0.195 (0.191) | 0.154 | 0.041 | 0.291 |
| YNiBi | 6.411 | 0.221 (0.219) | 0.156 | 0.065 | 0.398 |

MAIN CALCULATED RESULTS AND ANALYSIS

Half-Heusler ANiB (A=Ti, Hf, Sc, Y; B=Sn, Sb, Bi) forms a MgAgAs type of structure with space group $F43m$, where A, Ni, and B atoms occupy Wyckoff positions 4a (0, 0, 0), 4c (1/4, 1/4, 1/4), and 4b (1/2, 1/2, 1/2) positions, respectively. The experimental lattice crystal structures[40] are used to do our calculations, and the lattice constants a are listed in Table I. Here, we investigate the electronic structures of TiNiSn, HfNiSn, ScNiSb, YNiSb, ScNiBi and YNiBi with the 18 valence electron count (VEC) per unit cell by using GGA and GGA+SOC, and present their energy band structures in Figure 1. They are all indirect-gap semiconductors, with the conduction band minimum (CBM) at high symmetry point X and valence band maximum (VBM) at the Γ point. These gaps are produced due to the strong hybridization of d states of the A and Ni atoms. The valence bands near the Fermi level are dominated by the A-d state hybridized with the Ni-d and B-p states, while the bottom of the conduction bands are constructed mostly by A-d and Ni-d states. Based on our calculation, the GGA gap values vary from about 0.195 eV to 0.460 eV, and GGA+SOC ones change from 0.154 eV to 0.452 eV. Our GGA gap values are well consistent with other

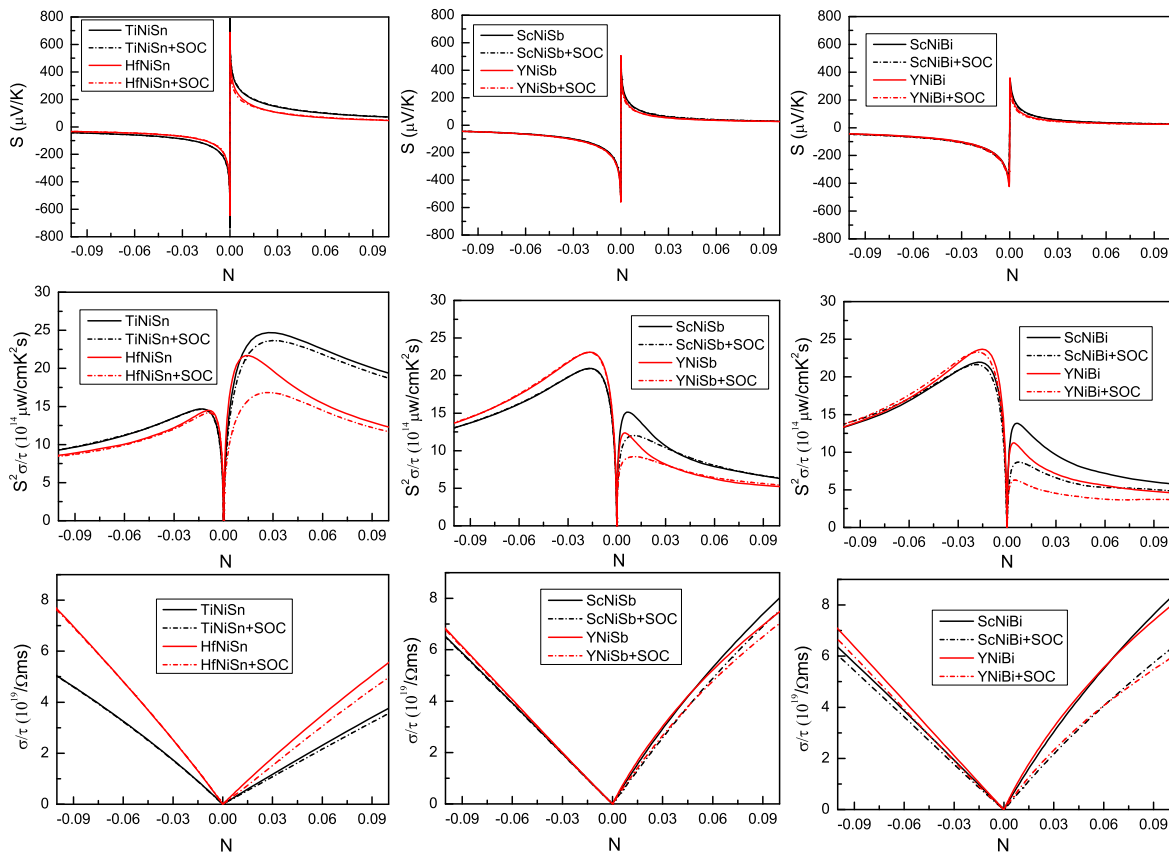


FIG. 3. (Color online) At temperature of 300 K, transport coefficients as a function of doping levels (electrons [minus value] or holes [positive value] per unit cell): Seebeck coefficient S (Top panel), power factor with respect to scattering time $S^2\sigma/\tau$ (Middle panel) and electrical conductivity with respect to scattering time σ/τ (Bottom panel) calculated with GGA (Solid line) and GGA+SOC (Dotted line).

theoretical values[26] calculated by using density functional projector augmented plane-wave method within the GGA. This SOC effect on gap strongly depends on A and B atoms, and the larger gap reduce means more obvious influence on conduction bands near Fermi level. We show the related gap values in Table I. To describe the SOC effects on the valence bands near Fermi level, spin-orbit splitting at the Γ point near the Fermi level in the valence bands are calculated, and are listed in Table I. These data show SOC has larger influence on the valence bands with respect to conduction bands.

Half-Heusler is considered as a kind of potential thermoelectric material for converting heat directly to electricity. The calculations of the semi-classic transport coefficients as a function of doping level are performed within constant scattering time approximation Boltzmann theory, and the temperature and doping dependence of the band structure are supposed to have a negligible effect on the transport coefficients. First, we plot the corresponding relation between the doping concentration and electrons or holes per unit cell in Figure 2, and it is natural that they have a linear relation. Figure 3 shows the Seebeck coefficient S , power factor with

respect to scattering time $S^2\sigma/\tau$ and electrical conductivity with respect to scattering time σ/τ as a function of doping levels at the temperature of 300 K by using GGA and GGA+SOC. To clearly see the difference of Seebeck coefficient between GGA and GGA+SOC, the enlargers near the gap are present in Figure 4. The negative doping levels imply the n-type doping with the negative Seebeck coefficient, and the positive doping levels mean p-type doping with the positive Seebeck coefficient.

It is clearly seen that these compounds containing Sn have larger Seebeck coefficient in p-type doping than in n-type doping, while it is totally contrary to those compounds containing Sb and Bi. Due to S being proportional to effective mass m^* , the analysis of the effective mass can explain the differences. From Figure 1, we can see that the VBM have larger effective mass than CBM for TiNiSn and HfNiSn, while the CBM of compounds containing Sb and Bi have larger one than VBM. (The CBM has a dominant contribution to thermoelectric properties in the case of n-type doping, while VBM for p-type doping.) Power factor with respect to scattering time $S^2\sigma/\tau$ changes in the same trend with Seebeck coefficient, and electrical conductivity with respect

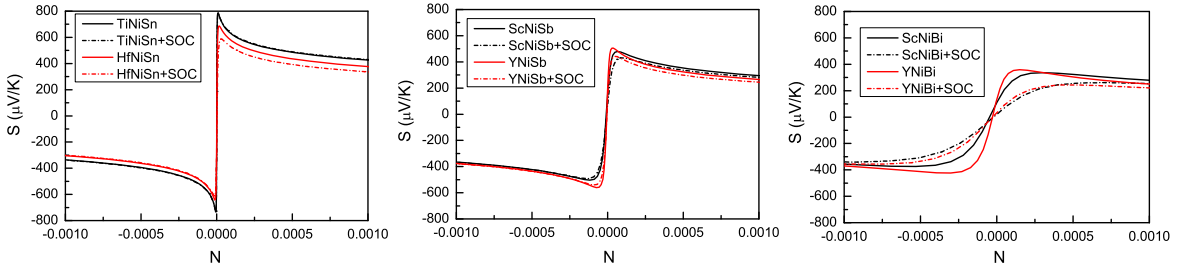


FIG. 4. (Color online) At temperature of 300 K, Seebeck coefficient S (enlarged near energy gap) as a function of doping levels (electrons [minus value] or holes [positive value] per unit cell) calculated with GGA (Solid line) and GGA+SOC (Dotted line).

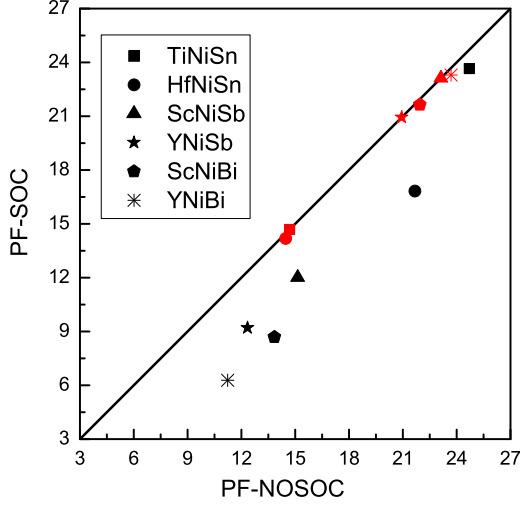


FIG. 5. (Color online) At temperature of 300 K, the maximal power factor for p-type doping (Black mark) and n-type doping (Red mark). The horizontal axis represents GGA values, and the vertical axis shows GGA+SOC values.

to scattering time σ/τ changes in the opposite trend simultaneously.

Calculated results show a negligible SOC effect on S , $S^2\sigma/\tau$ and σ/τ in n-type doping for the compounds containing Sn and Sb atoms. However, in p-type doping, a detrimental influence of SOC on the thermoelectric performance of the six kinds of compounds except the S of TiNiSn is observed. These can be understood by that SOC has larger effects on the valence bands near the Fermi level than the conduction bands. For ScNiBi and YNiBi, SOC has a observable detrimental influence on their thermoelectric performance in n-type doping, which is because they contain heavier Bi atom, although the Bi atom contributes a small weight to the conduction bands near the Fermi level. Finally, the maximum power factors (MPF) in unit of $\tau \times 10^{14} \mu W / (cm K^2 s)$ are extracted in n-type and p-type doping with GGA and GGA+SOC, and are plotted in Figure 5. It is obvious that SOC has little influences on n-type MPF, and has remarkable effects on p-type MPF. At temperature of 300 K, p-type TiNiSn have the largest power factor, followed by n-type

YNiBi and ScNiSb. We summarize related MPF calculated with GGA and GGA+SOC in p-type and n-type doping, the corresponding doping levels and other theoretical values in Table II. Our GGA MPF and the corresponding doping levels agree well with other calculated values[26].

DISCUSSIONS AND CONCLUSION

The SOC removes the band degeneracy, and the importance of SOC gradually increases with increasing atomic number of A and B atoms. The valence bands around the high symmetry Γ point can show obvious relativistic effects. The spin-orbit splitting removes the degeneracy of electronic states at Γ point, and modifies the outline of bands, which produces the remarkable effects on the p-type power factor. According to the spin-orbit splitting Δ in the Table I and the MPF in Table II, it is found that the larger Δ leads to the more obvious detrimental influence on p-type MPF. The MPF by using GGA+SOC in p-type doping is about 4.25%, 20.60%, 22.33%, 25.50%, 37.21% and 44.13% smaller than that with GGA for TiNiSn, ScNiSb, HfNiSn, YNiSb, ScNiBi and YNiBi, respectively, and their related spin-orbit splitting Δ also gradually increases from 0.025 eV to 0.398 eV. In fact, the power factor decay in n-type doping is connected to difference value between gap with GGA and gap with GGA+SOC ($E_1 - E_2$), and the larger gap difference value induces the larger decay.

In summary, GGA and GGA+SOC are chosen to investigate electronic structures and thermoelectric properties of half-Heusler ANiB (A=Ti, Hf, Sc, Y; B=Sn, Sb, Bi). The strength of SOC influences on valence and conduction bands near the Fermi level is shown by the related gaps Δ and $E_1 - E_2$. It is found that the power factors of p-doped TiNiSn and HfNiSn are much higher than the values attained in n-type doping, and it is opposite to half-Heusler compounds containing Sb and Bi elements. Calculated results show that the SOC is a significant factor decreasing the power factor of p-type ANiB, especially for ScNiBi and YNiBi. In p-type doping, the MPF reduce of YNiBi by using GGA+SOC is as much

TABLE II. The MPF in unit of $\tau \times 10^{14} \mu W / (cm K^2 s)$ and the corresponding doping levels (electrons [n-type] or holes [p-type] per unit cell) by using GGA and GGA+SOC. These values in the parentheses are GGA MPF in ref.[26].

| | | TiNiSn | HfNiSn | ScNiSb | YNiSb | ScNiBi | YNiBi |
|---------|----------|---------------|---------------|---------------|---------------|---------------|---------------|
| GGA | MPF(p) | 24.70 (25.13) | 21.67 (22.03) | 15.14 (15.82) | 12.35 (13.18) | 13.84 (14.54) | 11.24 (11.98) |
| | p doping | 0.027 (0.028) | 0.015 (0.014) | 0.007 (0.006) | 0.005 (0.005) | 0.006 (0.006) | 0.004 (0.004) |
| | MPF(n) | 14.68 (14.45) | 14.47 (14.44) | 23.13 (20.64) | 20.93 (22.83) | 21.95 (21.63) | 23.68 (23.44) |
| | n doping | 0.013 (0.013) | 0.009 (0.009) | 0.017 (0.016) | 0.015 (0.017) | 0.018 (0.016) | 0.015 (0.015) |
| GGA+SOC | MPF(p) | 23.65 | 16.83 | 12.02 | 9.20 | 8.69 | 6.28 |
| | p doping | 0.030 | 0.028 | 0.010 | 0.011 | 0.007 | 0.005 |
| | MPF(n) | 14.68 | 14.18 | 23.13 | 20.93 | 21.64 | 23.30 |
| | n doping | 0.013 | 0.008 | 0.017 | 0.015 | 0.018 | 0.019 |

as 44.13% with respect to GGA. So, it is very necessary for power factor calculations to consider SOC, when half-Heusler compounds are composed of heavy elements such as Bi or Sb.

This work is supported by the National Natural Science Foundation of China (Grant No. 11404391). We are grateful to the Advanced Analysis and Computation Center of CUMT for the award of CPU hours to accomplish this work.

- [1] Y. Pei, X. Shi, A. LaLonde, H. Wang, L. Chen, G. J. Snyder, *Nature* **473**, 66 (2011).
- [2] A. D. LaLonde, Y. Pei, H. Wang and G. J. Snyder, *Mater. Today* **14**, 526 (2011).
- [3] W. S. Liu, Q. Y. Zhang, Y. C. Lan, S. Chen, X. Yan, Q. Zhang, H. Wang, D. Z. Wang, G. Chen and Z. F. Ren, *Adv. Energy Mater.* **1**, 577 (2011).
- [4] D. K. Ko, Y. J. Kang and C. B. Murray, *Nano Lett.*, **11**, 2841 (2011).
- [5] M. Zebarjadi, et al. *Nano Lett.* **11**, 2225 (2011).
- [6] B. Yu, et al. *Nano Lett.* **12**, 2077 (2012).
- [7] Y. Z. Pei, X. Y. Shi, A. Lalonde et al, *Nature* **473**, 66 (2011).
- [8] J. Q. He, J. R. Sootsman, S. N. Girard et al, *J. Am. Chem. Soc.* **132**, 8669 (2010).
- [9] A. C. Sklad, M. W. Gaultois and A. P. Grosvenor, *J. Alloys Compd.* **505**, L6 (2010).
- [10] X. Shi, J. Yang and J. R. Salvador, *J. Am. Chem. Soc.* **133**, 7837 (2011).
- [11] T. Graf, C. Felser and Stuart S.P. Parkin, *Prog. Solid State Ch.* **39**, 1 (2011).
- [12] J. R. Sootsman, *Angew. Chem.* **48**, 8616 (2009).
- [13] M. Schwall and B. Balke, *Appl. Phys. Lett.* **98**, 042106 (2011).
- [14] F.G. Aliev, et al. *Z. Phys. B: Condensed Matter* **80**, 353 (1990).
- [15] I. Galanakis, et al. *Phys. Rev. B* **66**, 134428 (2002).
- [16] S. Chen and Z. F. Ren, *Mater. Today* **16**, 387 (2013).
- [17] J. Yang, et al. *Adv. Funct. Mater.* **18**, 2880 (2008).
- [18] J. W. Simonson and S. J. Poon, *J. Phys.: Condensed Matter* **20**, 255220 (2008).
- [19] D. J. Singh, *Semicond. Semimet.* **70**, 125 (2001).
- [20] G. K. H. Madsen, *J. Am. Chem. Soc.* **128**, 12140 (2006).
- [21] G. K. H. Madsen and D. J. Singh, *Comput. Phys. Commun.* **175**, 67 (2006).
- [22] G. Q. Ding, G. Y. Gao and K. L. Yao, *J. Phys. D: Appl. Phys.* **47**, 385305 (2014).
- [23] G. Li, K. Kurosaki, Y. Ohishi, H. Muta and S. Yamanaka, *Japan. J. Appl. Phys.* **52**, 041804 (2013).
- [24] S. Sharma and S. K. Pandey, *J. Phys.: Condens. Matter* **26**, 215501 (2014).
- [25] J. M. Mena, H. G. Schoberth, T. Gruhn and H. Emmerich, *J. Alloys Compd.* **650**, 728 (2015).
- [26] J. Yang, Z. G. Mei, L. Xi, W. Zhang and L. D. Chen, *Proceedings of International Symposium on EcoTopia Science 2007, ISETS07 (2007)*; J. Yang, H. M. Li, T. Wu, W. Q. Zhang, L. D. Chen and J. H. Yang, *Adv. Funct. Mater.* **18**, 2880 (2008).
- [27] M. ONOUE, F. ISHII and T. OGUCHI, *J. Phys. Soc. Jpn.* **77**, 054706 (2008).
- [28] M. Z. Hasan and C. L. Kane, *Rev. Mod. Phys.* **82**, 3045 (2010).
- [29] K. Kutorasinski, B. Wiendlocha, J. Tobola and S. Kaprzyk, *Phys. Rev. B* **89**, 115205 (2014).
- [30] P. Hohenberg and W. Kohn, *Phys. Rev.* **136**, B864 (1964); W. Kohn and L. J. Sham, *Phys. Rev.* **140**, A1133 (1965).
- [31] P. Blaha, K. Schwarz, G. K. H. Madsen, D. Kvasnicka and J. Luitz, WIEN2k, an Augmented Plane Wave + Local Orbitals Program for Calculating Crystal Properties (Karlheinz Schwarz Technische Universität Wien, Austria) 2001, ISBN 3-9501031-1-2
- [32] J. P. Perdew, K. Burke and M. Ernzerhof, *Phys. Rev. Lett.* **77**, 3865 (1996).
- [33] A. H. MacDonald, W. E. Pickett and D. D. Koelling, *J. Phys. C* **13**, 2675 (1980).
- [34] D. J. Singh and L. Nordstrom, *Plane Waves, Pseudopotentials and the LAPW Method*, 2nd Edition (Springer, New York, 2006).
- [35] J. Kunes, P. Novak, R. Schmid, P. Blaha and K. Schwarz, *Phys. Rev. B* **64**, 153102 (2001).
- [36] D. D. Koelling, B. N. Harmon, *J. Phys. C Solid State Phys.* **10**, 3107 (1977)
- [37] B. L. Huang and M. Kaviani, *Phys. Rev. B* **77**, 125209 (2008).
- [38] L. Q. Xu, Y. P. Zheng and J. C. Zheng, *Phys. Rev. B* **82**, 195102 (2010).
- [39] S. D. Guo, *EPL* **109**, 57002 (2015).
- [40] Inorganic Crystal Structure Database (ICSD).